IEEE Access
Multidisciplinary | Rapid Review | Open Access Journal

Received June 5, 2019, accepted July 9, 2019, date of publication July 11, 2019, date of current version August 1, 2019.

Digital Object Identifier 10.1109/ACCESS.2019.2928242

Analytical Prediction of the Radiation Characteristics of 2 × 2 Ridge Gap Waveguide Slot Antenna Array With Suppressed Grating Lobes at the V-band

HUSSEIN ATTIA, (Member, IEEE)
Electrical Engineering Department, King Fahd University of Petroleum and Minerals, Dhahran 31261, Saudi Arabia
e-mail: hattia@kfupm.edu.sa

This work was supported by the Deanship of Research at King Fahd University of Petroleum and Minerals (KFUPM) under Project IN161033.

ABSTRACT In this paper, the radiation patterns due to magnetic sources embedded in a ground plane in the presence of a partially reflective surface are analytically formulated and calculated. Love's equivalence principle, the transmission-line analogy, and the reciprocity theory are all combined and employed to calculate the far-fields of a four-element (2 × 2) slot array excited by the printed ridge gap waveguide technology operating in the V-band. Since the spacing between the array elements is greater than one wavelength, grating lobes cannot be avoided. Hence, to suppress the grating lobes and enhance the antenna directivity, a dielectric superstrate with the proper properties is utilized. The slot antenna array is operating at 60 GHz for millimeter-wave applications. The obtained results from the proposed analytical formulation agree very well with full-wave numerical simulations obtained from the EM commercial tool HFSS. It is worthwhile to mention that the presented analytical solution is about 30 times faster than its full-wave simulator counterpart.

INDEX TERMS Ridge gap, slot array, magnetic sources, partially reflective surface, grating lobes.

I. INTRODUCTION

Recently, considerable interest has been focused on high-gain radiating systems at the V-band (40 – 75 GHz) for indoor and point-to-point wireless communication. Specifically, the interest has increased in the frequency range between 57 and 64 GHz after the Federal Communications Commission (FCC) declared this as an unlicensed band for wireless systems.

The use of superstrate(s) above planar antennas has been widely used to enhance their directivity [1]–[10]. The gain of a printed Hertzian dipole has been improved significantly to about 21 dB after using a quarter-wavelength thick superstrate and achieving appropriate resonance conditions [2], these resonance conditions require having a superstrate with very high dielectric constant (i.e., $\varepsilon_r = 100$) or very high relative permeability (i.e., $\mu_r = 100$). These resonance conditions, seemingly to be impractical in the recent past, can be realized presently using a variety of contemporary metamaterial structures [11]–[16]. In [3], the finite sizes of the ground plane and dielectric superstrate have been found to have a major effect on the antenna aperture efficiency that may exceed 100% when the superstrate's diameter is less than 1.2λ; where λ is the free-space wavelength. In [4], the concept of superstrate above planar antennas has been utilized with a waveguide aperture surrounded by a finite size flange. The effect of multilayer dielectric superstrates was generalized in [5] when the superstrates are terminated by inductive terminators in addition to inserting layers of two-dimensional striplines polarizers. In [6], an engineered (i.e., artificial) magnetic material based on split ring resonator (SRR) has been placed over a microstrip antenna to enhance its radiation properties, the antenna directivity has increased by 3.5 dB while preserving a small profile of the whole radiating system. In [7], a metamaterial-based lens has been used as a superstrate in the Ka-band to enhance the gain of a magneto-electric dipole

The associate editor coordinating the review of this manuscript and approving it for publication was Nagendra Prasad Pathak.

antenna, and the antenna was excited through an aperture coupled to a fork-shaped ridge gap waveguide. A 60 GHz wideband high-gain antenna was presented in [8], where a frequency-selective surface (FSS) has been employed to act as a partially reflective surface (PRS) above a slot antenna excited by printed ridge gap waveguide technology (PRGW).

The authors in [9] have employed an FSS-based perforated conductive sheet as a superstrate above a slot-dipole antenna operating in the V-band, thus creating a Fabry–Pérot cavity resonator, the obtained 3-dB gain bandwidth was 61-65 GHz (i.e., 6.3%).

Other methods to achieve high gain antennas exist, such as using large-scale arrays. Although planar antenna arrays have smaller volume than antennas with superstrates, they need a sophisticated feeding network that introduces losses and increases the structure footprint [17], [18].

In this work, I present, for the first time in literature, the analytical formulation for the radiation patterns due to magnetic sources embedded in a ground plane in the presence of a partially reflective surface (PRS). The transmission-line (T.L.) model, the reciprocity theory, and the equivalence principle are all combined and employed to calculate the far-fields of a 2 × 2 slot antenna array fed by PRGW technology and loaded by dielectric superstrate acting as a PRS at 60 GHz. Reduced propagation losses and planar geometry are the two main advantages of the PRGW feeding method [19]–[22]. The work in [22] presented preliminary simulated results on the application of PRGW to feed a slot antenna array, HFSS was used to produce the obtained preliminary results.

The application of PRGW at V-band has shown attractive wideband behavior and good radiation patterns when integrated with slot-based arrays [20]. The major drawback of using such a feeding mechanism (i.e., PRGW) is in its demand for high computational resources. Thus, the analytical technique proposed here helps in significantly speeding up the simulation process and in reducing the computational requirements significantly without compromising the results accuracy.

It is desirable to reasonably increase the distance between the array elements, which reduces the mutual coupling between them [23]. However, if the distance between the elements exceeds the wavelength, grating lobes are created. Using the PRGW technology feeding network make it challenging to place the array elements closer than one wavelength at 60 GHz [24]. An inexpensive solution to decrease the grating lobes of the PRGW antenna array and enhance the broadside directivity is to use a low-cost dielectric lens. One of the simplest lenses is the planar PRS parallel to the array ground plane, which enhances the antenna directivity and reduces the grating lobe level.

The author of this work emphasizes that the main *objective* of this work is introducing a fast and highly-efficient analytical solution for the far fields of an antenna array fed by PRGW operating at 60 GHz, the obtained analytical results are verified by full-wave numerical simulations.

This paper is organized as follows: in section II, the design and analysis of a PRGW 2 × 2 slot-antenna array covered with a partially reflective surface are presented. Section III introduces the proposed analytical formulation for computing the radiation fields of the PRGW antenna array. Section IV depicts the validation of the obtained analytical results with full-wave numerical results. Finally, major accomplishments and conclusion are presented in section V.

II. 2 × 2 PRGW-FED SLOT ANTENNA ARRAY LOADED WITH A PRS

It was firstly demonstrated in [1] that the employment of a PRS above a primary radiating source (i.e., antenna) close to a ground plane increases the gain significantly. It was later shown in [2] that certain resonance conditions need to be satisfied to achieve such a significant increase in the antenna gain and directivity. These resonance conditions include the proper choice of the PRS thickness, its permittivity and permeability, and the spacing between the antenna and the PRS.

The brief analytical formulation concisely introduced in [25] for a single slot antenna is generalized and extended in this work to calculate the radiation patterns of 2 × 2 slot antenna array excited by ridge gap waveguide technology and imbedded in a multilayered structure to improve the antenna gain and decrease the side-lobes level. The PRGW technology as a low-loss feeding mechanism of the antenna array at 60 GHz will be elaborated in the following sub-sections.

A. PRINTED RIDGE GAP WAVEGUIDE (PRGW)

In PRGW technology [7], [8], [19]–[22] as depicted in Figs.1-2, the propagating electromagnetic waves are confined between two parallel surfaces, one surface is a PEC denoted as PRGW top plate and the other surface is a perfect magnetic conductor (PMC). Fig. 1 depicts the top view of the feeding network of the four-element slot array antenna created on the bottom PMC surface (i.e., mushroom surface) of the PRGW structure, note that only half of the symmetrical structure is shown in Fig. 1. The top PEC plate of the PRGW (see Fig. 2) is a thin copper plate and the bottom plate is realized as a texture 2D mushroom structure to mimic a PMC. The unit cell of the mushroom structure is a metallic circular patch connected to the ground plane by a

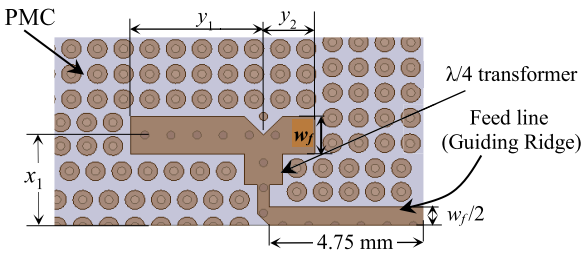

FIGURE 1. Top view of the feed network of the 2 × 2 slot antenna array created in the PRGW top-plate (only half of the symmetrical structure is shown).

metal-plated via. This unit cell whose dimensions are shown in Fig. 2 is designed using a substrate of Rogers 3003 with a dielectric constant of 3 and 0.5 mm thickness. The unit cell was optimized using CST Eigen-mode solver by changing the periodicity of the unit cell, the diameter of the circular patch, and the air gap height. The obtained dispersion diagram is depicted in Fig. 3, a band-gap between 53 and 100 GHz has been achieved to establish a PMC structure. This PMC will prevent any wave leakage from the array feed network [8]. The insertion of a guiding ridge (i.e., feed line) in the middle of the PMC plate will excite a quasi-TEM propagating mode that is needed to feed the antenna array. Through plated holes (i.e., vias) are utilized to connect the feeding lines to the ground plane to mitigate any EM waves propagating underneath the feeding lines or inside the PMC substrate [8]. Moreover, this will restrict the wave propagation along the feeding network. The accomplished band-gap of 53 to 100 GHz is more than the required bandwidth of the targeted 60 GHz four-element slot antenna array.

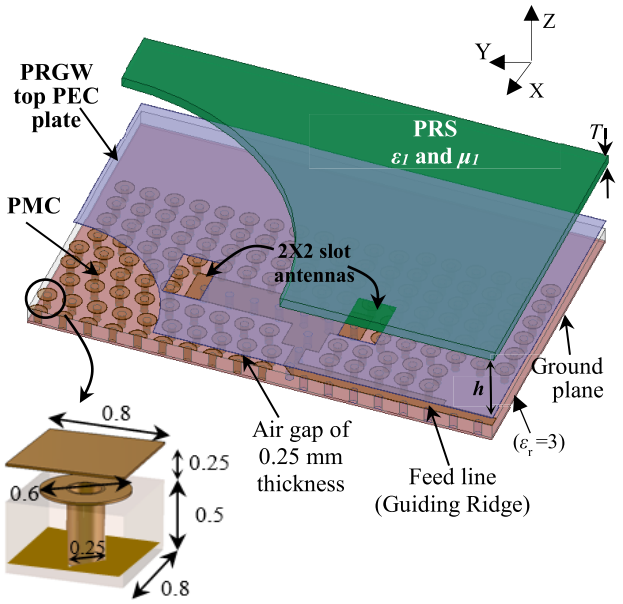

FIGURE 2. Perspective view of the PRGW slot antenna array loaded with a PRS of thickness (*T*) at distance (*h*) in the air. The top plate and the PRS are partly removed to show the details under them. All dimensions are in mm. (only half of the symmetrical structure is shown).

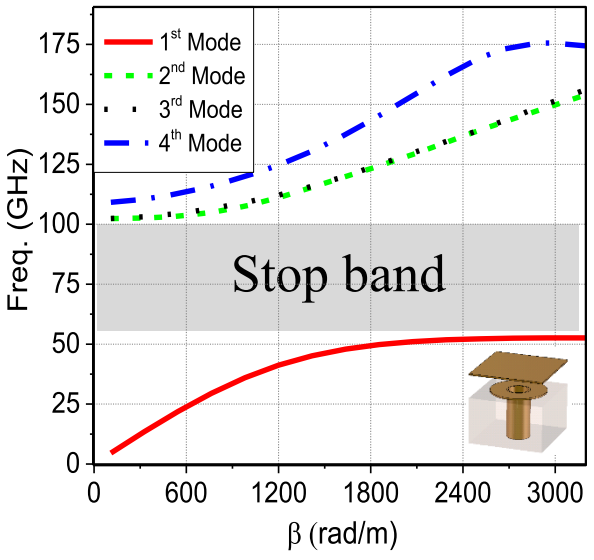

FIGURE 3. Dispersion graph of the mushroom structure unit-cell employed to create the required stop band of 53-100 GHz.

The PRGW top PEC plate is placed at a small distance of 0.25 mm above the PMC plate to allow wave propagation only along the feed network and to provide the desired stop-band for parallel plates mode. The presence of the mushroom structure (i.e., PMC) is intended to prohibit any wave leakage from the feed network and therefore greatly decreases radiation losses in the frequency band of interest [8].

The characteristic impedance of the main feed line (guiding ridge) shown in Figs.1 and 2 is determined by the thickness of the air-gap between the bottom PMC and the top PEC plate (i.e., 0.25 mm) and by the width of the ridge line (w_f) itself, this width has been optimized to exhibit a 50-Ω characteristic impedance. The characteristic impedance of the ridge line will vary slightly with frequency because it supports Quasi-TEM modes [26]. This was studied and investigated in [19]–[20] which showed that conventional definition for microstrip lines gives a satisfactory accuracy for obtaining the characteristic impedance of PRGW ridge lines. The chosen width (w_f) and length of the main feeding line (guiding ridge) are 1.2 mm and 4.75 mm, respectively. This value of (w_f) is the average value of the line width when it is printed on the RO3003 material and when it is printed on air (i.e., gap) substrate since the propagation of the wave along the line is affected by both substrates (i.e., RO3003 and air gap). Regarding the length of this line, it is chosen based on the desired size of the whole antenna array and it affects the shape of the radiation patterns as well, more sidelobes would appear for longer feeding line due to the undesired radiation from this line. It is worth pointing out that the air-gap separation between the PMC and PEC top plate is the propagation medium and its thickness is equal to 0.25 mm which is much lower than quarter-wavelength at the operating frequency of 60 GHz.

B. 2 × 2 ANTENNA ARRAY FED BY PRGW

The array feeding network shown in Fig. 1 is designed as a parallel feeding network that requires inserting quarter-wavelength transformers to provide the necessary matching. Fig. 2 depicts the 3-D view of the slot antenna array based on the PRGW and covered with a dielectric PRS of thickness (T) and placed at a distance (h) in the air above the slot antenna array.

A four-element 2 × 2 slot array is created in the PRGW top PEC plate. Through parametric analysis in HFSS, the slot dimensions of 1.9 × 1.2 mm^2 were obtained to enable the slot to radiate at the millimeter-wave frequency band of about 57 to 64 GHz. The slot length of 1.9 mm is comparable to a

half free-space wavelength at 60 GHz since the slot antenna is a dual of a patch antenna where the conductive patch is replaced by air. To reduce the coupling effects between the four elements, they are positioned slightly more than one free-space wavelength apart from one another. The dimensions shown in Fig. 1 (i.e., $x_1 = 2.875$ mm, $y_1 = 4.06$ mm, and $y_2 = 1.56$ mm) determine the spacing between the array elements. The employed $\lambda/4$ transformer is of dimensions 0.98x1.2 mm^2 to provide the necessary matching. The antenna array is loaded with a PRS of thickness (T) and a dielectric constant and relative permeability of ε_1 and μ_1, respectively. The proposed analytical analysis of this antenna array is discussed in the following section then validated by full-wave numerical simulations in Section IV.

III. ANALYTICAL FORMULATION OF FAR-FIELDS of PRGW ANTENNA ARRAY WITH SUPERSTRATE

The radiated far field of the PRGW-fed slot antenna array can be calculated using Love's equivalence principle, T.L. analogy and the reciprocity theorem. Fig. 4 shows the side view of an aperture rectangle slot of dimensions ($a \times b$) embedded in a ground plane (PRGW top plate). A PRS of thickness (T) and refractive index of $n_1 = \sqrt{\varepsilon_1 \mu_1}$ covers this single slot antenna at a distance (h) in order to improve the radiation characteristics. Based on Love's equivalence principle [27], the assumed y-polarized electric field (E_a) of the rectangular aperture will induce an equivalent magnetic current source of

$$M_s = -\hat{n} \times E_a \tag{1}$$

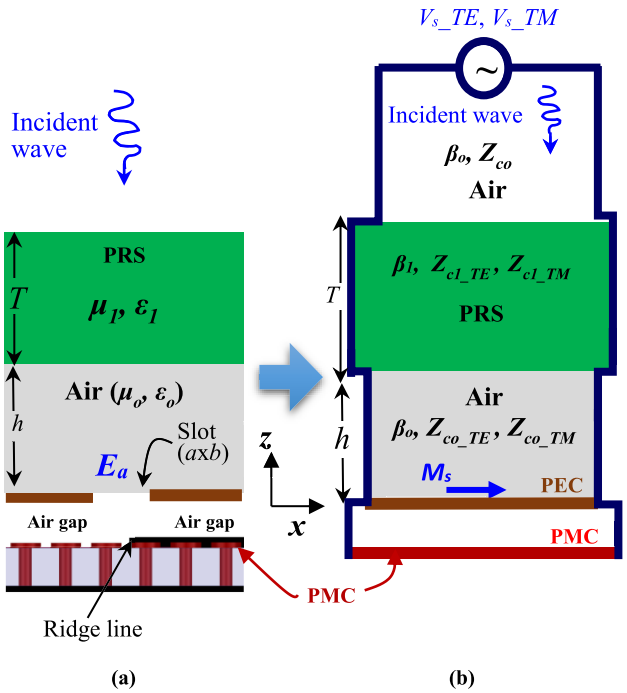

FIGURE 4. (a) PRGW-fed rectangular aperture (i.e., slot) radiating electric field Ea embedded in a ground-plane and loaded with a PRS of μ_1 and ε_1. (b) T.L. modeling of the entire radiating system.

This magnetic current source is essentially very near to the PRGW top PEC plate (assume $\hat{n} = \hat{a}_z$ which is the normal unit vector on the aperture plan). From (1), the equivalent magnetic current source will be x-polarized. Hence, the sought radiated electric far-field (E) at an arbitrary test point P (r, θ, $\emptyset$) will be obtained due to this magnetic current density (M_s) located at the slot. The reciprocity theorem is then used to find this radiated electric field (E). A very small-dipole J with length $\leq \lambda/50$ (reciprocity antenna) that is assumed at the test point emits a magnetic field (H) at the considered location of the slot antenna. Hence, the far-field (E) radiated from this slot, can be formulated as follows:

$$\iiint_V M_s \cdot H \, dV = -\iiint_V J.E \, dV \tag{2}$$

Assuming the reciprocity source to have a value of

$$J = \delta(\vec{r} - \vec{r}_p)\,\hat{u} \tag{3}$$

where ($\hat{u} = \hat{\theta}$ and $\hat{\varphi}$ for TM and TE incident waves, respectively). Hence, Equation (2) can be written as:

$$E(r_p).\hat{u} = -\iiint_V M_s \cdot H \, dV \tag{4}$$

From (4), the radiated field (E) at P (r, θ , $\emptyset$) can be calculated after determining the magnetic field (H) from the reciprocity source at the slot's position due to the reciprocity dipole. Since H is a plane-wave, it could be calculated using the T.L. modeling by considering the multilayered air-PRS structure (see Fig. 4) as interconnected T.L. sections loaded by a short circuit (i.e., ground plane). The characteristic impedance (Z_c) and propagation constants (β) of the different sections of the T.L. model can be formulated from the oblique incidence of a plane-wave at the interface of two dielectrics [26].

The effective refractive index which is dependent on the angle of incidence (θ) in the air and PRS layers, can be defined as

$$n_o(\theta) = \sqrt{n_0^2 - sin^2(\theta)} \quad \text{(air layer)} \tag{5}$$

$$n_1(\theta) = \sqrt{n_1^2 - sin^2(\theta)} \quad \text{(PRS layer)} \tag{6}$$

where $n_o = \sqrt{(\varepsilon_r \mu_r)_{air}}$ and $n_1 = \sqrt{\varepsilon_1 \mu_1}$ are the indexes of refraction in the air and PRS layer, respectively.

Hence, the definitions of β in the air and PRS layers can be defined as

$$\beta_o(\theta) = K_o n_o(\theta) \quad \text{(air layer)} \tag{7}$$

$$\beta_1(\theta) = K_o n_1(\theta) \quad \text{(PRS layer)} \tag{8}$$

For transverse electric (TE) wave or perpendicular polarization, the characteristic impedances of the air and PRS layers can be defined as:

$$Z_{co}^{TE}(\theta) = \frac{\eta_o}{n_0(\theta)} \quad \text{(air layer)} \tag{9}$$

$$Z_{c1}^{TE}(\theta) = \frac{\eta_o \mu_1}{n_1(\theta)} \quad \text{(PRS layer)} \tag{10}$$

For transverse magnetic (*TM*) wave or parallel polarization, the characteristic impedances of the air and PRS layers can be defined as:

$$Z_{co}^{TM}(\theta) = \eta_o n_0(\theta) \quad \text{(air layer)} \tag{11}$$

$$Z_{c1}^{TM}(\theta) = \frac{\eta_o n_1(\theta)}{\varepsilon_1} \quad \text{(PRS layer)} \tag{12}$$

In the above definitions of β , K_0 is the propagation constant in free-space for perpendicular incidence ($\theta = 0$) and equals to $\omega\sqrt{\mu_o\varepsilon_o}$, and η_o is the intrinsic impedance of free-space (i.e., the wave impedance of a plane-wave in free-space) and equals to $\sqrt{\mu_o/\varepsilon_o} = 377$ ohm.

For the *TE* wave radiated by the reciprocity infinitesimal dipole $J = \delta(\vec{r} - \vec{r}_p)\,\hat{\phi}$ that is placed at the test far point $P(r, \theta, \emptyset)$, this source would produce magnetic vector potential (A) in phi direction which in turn produces far electric field in same direction (i.e., phi) and magnetic field H in theta direction. Hence, the x-component of the H field radiated by the reciprocity source at the location of M_s can be expressed as

$$H_x = \cos(\phi)F(\theta)\left[\frac{e^{-JK_o r}}{r}\frac{JK_o}{4\pi}e^{JK_o(x'\sin(\theta)\cos(\phi)+z'\cos(\theta))}\right] \tag{13}$$

The function $F(\theta)$ depending only on θ represents the electric current at the slot's location ($z = 0$) in the T.L. analogy (see Fig. 4) due to an incident current wave of magnitude $\cos(\theta)$. The current at $z = 0$ can be computed by solving the following set of simultaneous equations using the Symbolic Math Toolbox™ in MATLAB [28],

$$\begin{aligned}
V_1 &= V_1^+ e^{-j\beta_0 z} + V_1^- e^{j\beta_0 z}\\
V_2 &= V_2^+ e^{-j\beta_1 z} + V_2^- e^{j\beta_1 z}\\
V_3 &= V_3^+ e^{-j\beta_0 z} + V_3^- e^{j\beta_0 z}\\
I_1 &= 1/Z_{c0}^{TE}(V_1^+ e^{-j\beta_0 z} - V_1^- e^{j\beta_0 z})\\
I_2 &= 1/Z_{c1}^{TE}(V_2^+ e^{-j\beta_1 z} - V_2^- e^{j\beta_1 z})\\
I_3 &= 1/Z_{c0}^{TE}(V_3^+ e^{-j\beta_0 z} - V_3^- e^{j\beta_0 z})
\end{aligned} \tag{14}$$

where (V_1, I_1) are the voltage and current in the bottom air layer right above the magnetic current source M_s, and (V_2, I_2) are the voltage and current in the PRS layer. (V_3, I_3) are the voltage and current in the top air layer.

The above equation set contains six unknowns that can be reduced to four unknowns using the facts that $V_1^- = -V_1^+$ due to the presence of ground plane at $z = 0$, and the justified assumption that $V_3^+/Z_{c0}^{TE} = \cos(\theta)$. The remaining four unknowns can be computed by the continuity of voltage and current at the interface between each two layers as depicted in Fig. 4. Hence, the function $F(\theta)$ will equal to $I_1(z = 0)$ that can be computed from (14).

For the *TM* wave radiated by the reciprocity infinitesimal dipole $J = \delta(\vec{r} - \vec{r}_p)\hat{\theta}$ that is placed at the test far point $P(r, \theta, \emptyset)$, this source would produce magnetic vector potential (A) in theta direction which in turn produces far electric field in same direction (i.e., theta) and magnetic field H in phi direction. Hence, the x-component of the H field radiated by the reciprocity source at the location of M_s can be expressed as

$$H_x = -\sin(\phi)G(\theta)\left[\frac{e^{-JK_o r}}{r}\frac{JK_o}{4\pi}e^{JK_o(x'\sin(\theta)\cos(\phi)+z'\cos(\theta))}\right] \tag{15}$$

The function $G(\theta)$ depending only on θ represents the electric current at the slot's location ($z = 0$) in the T.L. analogy (Fig. 4) due to an incident current wave of magnitude unity. This current can be computed employing the same technique used for the *TE* case. In other words, Eqs. (14) are to be re-written after replacing Z_{co}^{TE} by Z_c^{TM} and having $V_3^+/Z_{c0}^{TM} = 1$.

Using (4), the sought far-fields of the rectangular aperture is computed at the frequency of interest in both directions of theta and phi, and then numerically integrated to calculate the slot antenna directivity as:

$$D(\theta, \varphi) = \frac{4\pi * I}{\int_0^{\pi/2}\int_0^{2\pi} I \sin(\theta)\, d\varphi d\theta} \tag{16}$$

where,

$$I = \sin^2(X)/X^2 \sin^2(Y)/Y^2 * \begin{pmatrix} \cos^2\varphi |F(\theta)|^2 \\ +\sin^2\varphi |G(\theta)|^2 \end{pmatrix} \tag{17}$$

where $X = \frac{K_o a}{2}\cos\varphi\sin\theta$, $Y = \frac{K_o b}{2}\sin\varphi\sin\theta$
where (a, b) are the width and length of the rectangular slot aperture in x and y directions, respectively.

Considering the PRGW 2 × 2 slot antenna array shown in Fig. 2, its far-fields can be calculated at the desired frequency by multiplying (4) by the array factor (*AF*), which is mainly dependent on the spatial configuration of the planar array considered here [23]. Note that the progressive phase shift between the array elements is zero in both x and y directions. Hence, the directivity of the 2 × 2 slot antenna array shown in Fig. 2 is given by:

$$\begin{aligned}
D(\theta, \varphi) &= \frac{4\pi * I * |AF|^2}{\int_0^{\pi/2}\int_0^{2\pi} I * |AF|^2 \sin(\theta)\, d\varphi d\theta}\\
AF &= 2\cos(k_o x_1 \sin(\theta)\cos(\varphi))\\
&\quad * \begin{pmatrix} e^{(-jk_o y_1 \sin(\theta)\sin(\varphi))} \\ +e^{(jk_o y_2 \sin(\theta)\sin(\varphi))} \end{pmatrix}
\end{aligned} \tag{18}$$

where x_1, y_1, and y_2 are design parameters of the 2 × 2 feed network shown in Fig. 1 and given by:

$x_1 = 2.875$ mm, $y_1 = 4.06$ mm, and $y_2 = 1.56$ mm

IV. ANALYTICAL RESULTS AND VALIDATION WITH NUMERICAL SIMULATIONS

The main goal of this work is to provide a fast analytical formulation of the radiating system composed of a dielectric superstrate (i.e., PRS) above PRGW slot antenna array at 60 GHz. This structure is intended to enhance the antenna gain and reduce the grating lobes. To validate the proposed analytical formulation, different dielectric PRSs with different dielectric constants have been employed above the four-element PRGW antenna array. In all cases, the PRS thickness (T) is chosen to be $\lambda/4$ ($\lambda = \lambda_o/\sqrt{\varepsilon_1}$) at the resonance frequency of 60 GHz as per the resonance conditions

given in [2]. The PRS is placed at a distance (h) of half wavelength in the air (i.e., 2.5 mm at 60 GHz) above the slot antenna array as shown in Fig. 2. According to optical ray analysis introduced in [1], some the EM energy emitted by the antenna array will be reflected by the air-PRS interface based on Snell's law, wherein some of this EM energy will be transmitted through the PRS. The proper choice of the PRS parameters (i.e., thickness, dielectric constant, reflection magnitude and phase .... etc.) and the spacing (h) between the antenna and the PRS will allow the emitted rays through the PRS to deflect in a predetermined direction. Therefore, resonance conditions can be proposed to ensure a very large gain and directivity along the desired direction [2], [3]. These resonance conditions necessitate the PRS thickness to be a quarter dielectric wavelength and to be placed at a half free-space wavelength above the slot antenna, and the permittivity of the PRS to be very high.

The analytical model developed in the previous section is employed here to predict the behavior of the PRGW slot antenna array shown in Fig. 2. The obtained results from the developed model (Eqs. 1-18) were compared against those obtained from modeling the same structure using the EM software *High Frequency Structure Simulation* (HFSS). Figs.5-8 show the radiation patterns of the 2 × 2 PRGW slot antenna array covered with a PRS of $\varepsilon_1 = 1$, 3.66, 6.15 and 10.2, respectively, at 60 GHz. Very good agreement is obtained in the four cases between the proposed analytical model and HFSS. Since the array factor concept was used to calculate the far-fields of the antenna array, *mutual coupling* between the array elements was not accounted for and consequently some discrepancy is expected between the calculated and the simulated patterns. This discrepancy is more prominent in the E-plane (i.e., yz plane as seen in Fig. 2) due to the existence of the main feed line (ridge) along y-axis which enlarges the unavoidable coupling between the array elements. At high elevation angles, a small discrepancy between the two methods is observed. This is conceived to be due to the presumption of an infinite 2D planar structure in the T.L. modeling. Consequently, the calculations of the radiation in the lower hemisphere are not feasible due to the assumption of an infinite ground plane.

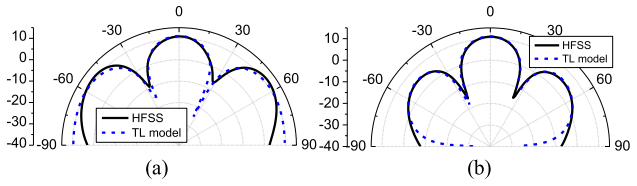

FIGURE 5. The directivity patterns at 60 GHz of the PRGW slot antenna array without a PRS (i.e., $\varepsilon_1 = 1$). (a) E-plane and (b) H-plane.

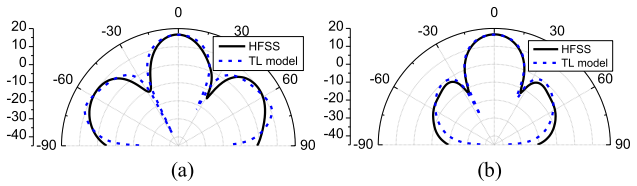

FIGURE 6. The directivity patterns at 60 GHz of the PRGW slot antenna array loaded with a PRS of $\varepsilon_1 = 3.66$. (a) E-plane and (b) H-plane.

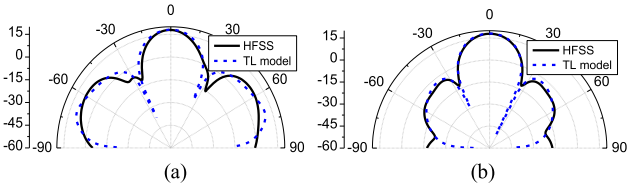

FIGURE 7. The directivity patterns at 60 GHz of the PRGW slot antenna array loaded with a PRS of $\varepsilon_1 = 6.15$. (a) E-plane and (b) H-plane.

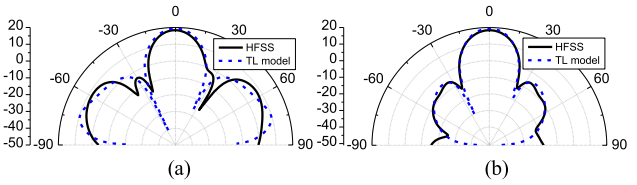

FIGURE 8. The directivity patterns at 60 GHz of the PRGW slot antenna array loaded with a PRS of $\varepsilon_1 = 10.2$. (a) E-plane and (b) H-plane.

Moreover, Figs.5-8 show an increase in the array directivity along the broadside direction with the increase of dielectric constant of the PRS. This directivity increase is depicted in Fig. 9; this figure is produced based on the results of Figs.5-8. Moreover, Fig. 9 shows that the rate of increase of the array directivity is higher with lower dielectric constant materials. It should be noted that the time taken by the proposed technique to calculate any of the patterns shown in Figs.5-8 is 3.9 minutes compared with 117 minutes when using HFSS.

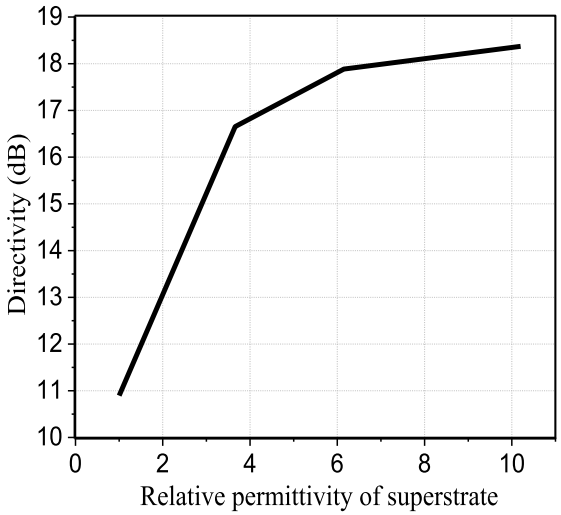

FIGURE 9. The directivity of the 2 × 2 PRGW slot array at 60 GHz for different PRS materials with different relative permittivities.

Fig. 10 shows the reflection coefficient and the directivity of the proposed array covered with a PRS of a dielectric

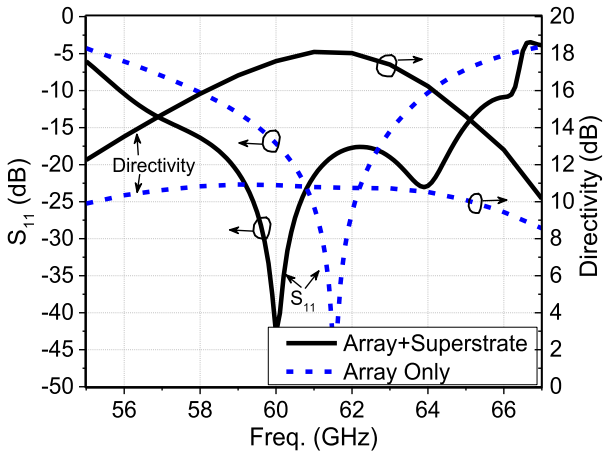

FIGURE 10. The reflection coefficient and directivity of the slot antenna array with and without a dielectric PRS of $\varepsilon_1 = 6.15$.

constant of 6.15. A 7.2 dB enhancement in the array directivity at 61 GHz and a 6% increase in the matching bandwidth are obtained. It is worth mentioning that this enhanced directivity (i.e., 18 dB at 61 GHz) can only be achieved by using 4×4 slot array without PRS, but with higher grating lobes. Moreover, the enhanced impedance bandwidth is achieved by the proper design of the slot parameters and the ridge guide dimensions and its position underneath the slot.

Figure 11 depicts the directivity patterns of the 2×2 PRGW slot antenna array *with and without* a dielectric PRS of $\varepsilon_1 = 6.15$ at 60 GHz. It is clear that the PRS reduces the grating lobe levels significantly in the H-plane. For the array with PRS, the H-plane grating lobe level at $\theta = 45^o$ is 24 dB below the main lobe level compared to 6 dB for the array without PRS. On the other hand, the E-plane pattern shows a grating lobe level of 11.5 dB below the main lobe level of the array with PRS compared with 1 dB for the array only. Note that the results in Fig. 11 are verified by the T.L. model as shown in Figs. 5 and 7.

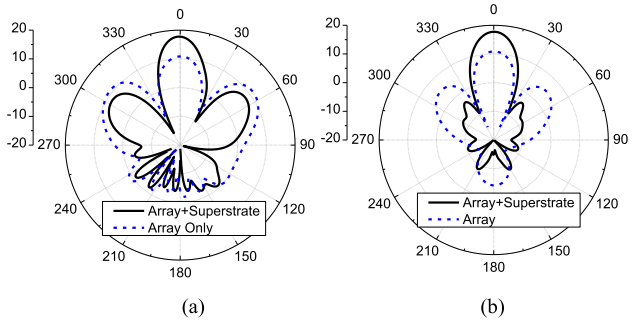

FIGURE 11. The directivity patterns of the PRGW 2 × 2 slot antenna array with and without a dielectric PRS of$\varepsilon 1 = 6.15$ at 60 GHz. (a) E-plane and (b) H-plane.

As the array impedance bandwidth is ranging from 56 to 66.2 GHz after using the PRS (see Fig. 10); it is necessary to show the radiation patterns at other frequencies within

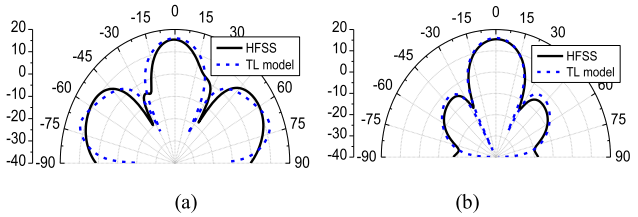

FIGURE 12. The directivity patterns of a 2 × 2 PRGW slot antenna array loaded with a dielectric PRS of $\varepsilon_1 = 6.15$ at 57 GHz. (a) E-plane and (b) H-plane.

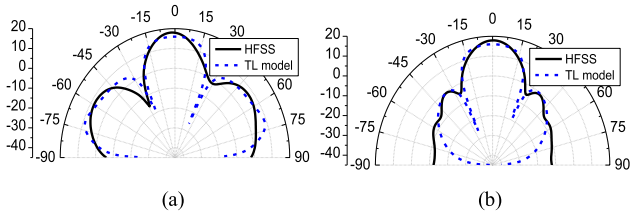

FIGURE 13. The directivity patterns of a 2 × 2 PRGW slot antenna array loaded with a dielectric PRS of $\varepsilon 1 = 6.15$ at 63 GHz. (a) E-plane and (b) H-plane.

this bandwidth. Figs.12 and 13 show the radiation patterns at 57 and 63 GHz, respectively, when using a PRS with dielectric constant of 6.15. It is apparent that the radiation pattern is consistent all over the antenna bandwidth. Also, the agreement between the T.L. model and HFSS is appreciable.

Though the analytical model proposed in this paper is not competent to calculate the antenna reflection coefficient, it is indeed a very *quick* and *efficient* technique to optimize the antenna's structure to achieve the desired far-field characteristics and to predict the antenna directivity and the shape of the radiation patterns for different structural parameters. The proposed technique can be merged smoothly with any optimization tool (i.e., genetic algorithm) to further optimize the array parameters. Afterwards, HFSS can be employed to calculate impedance bandwidth and to verify the calculated far-fields.

V. CONCLUSION

This work presents a very fast and highly-efficient analytical formulation that can predict the radiation fields of any planar antenna embedded in a multilayered structure. The antenna under consideration should be modeled as electric and/or magnetic current sources. As a case study, a PRGW excited slot antenna array loaded with a PRS superstrate has been considered to validate the proposed analytical formulation. This formulation is based on Love's equivalence principle, the reciprocity theory and the transmission-line model of the antenna-air-superstratemultilayered structure. The proposed analytical solution is about thirty times faster than its counterpart full-wave analysis. Moreover, the proposed formulation can easily be extended to analyze different types of FSS-based superstrate. The employment of the superstrate above the antenna array increases the antenna directivity by

more than 66% and consequently reduced the grating lobes associated with the antenna array. The proposed analytical solution is consistently accurate through the whole 56 to 66.2 GHz impedance bandwidth of the considered four-element antenna array.

ACKNOWLEDGMENT

This work was sponsored by the Deanship of Research at King Fahd University of Petroleum and Minerals (KFUPM) through project number IN161033. The author expresses his appreciation to Professor Ahmed Kishk from Concordia University, Montreal, Canada for the productive technical discussions and recommendations during the preparation of this paper.

REFERENCES

[1] G. V. Trentini, "Partially reflecting sheet arrays," *IRE Trans. Antennas Propag.*, vol. AP-4, no. 4, pp. 666–671, Oct. 1956.
[2] D. R. Jackson and N. Alexopoulos, "Gain enhancement methods for printed circuit antennas," *IEEE Trans. Antennas Propag.*, vol. AP-33, no. 9, pp. 976–987, Sep. 1985.
[3] A. A. Kishk and L. Shafai, "Gain enhancement of antennas over finite ground plane covered by a dielectric sheet," *IEE Proc. H-Microw., Antennas Propag.*, vol. 134, no. 1, pp. 60–64, Feb. 1987.
[4] A. A. Kishk, "One-dimensional electromagnetic bandgap for directivity enhancement of waveguide antennas," *Microw. Opt. Technol. Lett.*, vol. 47, no. 5, pp. 430–434, 2005.
[5] X. H. Wu, A. A. Kishk, and A. W. Glisson, "A transmission line method to compute the far-field radiation of arbitrary hertzian dipoles in a multilayer structure embedded with PEC strip interfaces," *IEEE Trans. Antennas Propag.*, vol. 55, no. 11, pp. 3191–3198, Nov. 2007.
[6] H. Attia, L. Yousefi, and O. M. Ramahi, "Analytical model for calculating the radiation field of microstrip antennas with artificial magnetic superstrates: Theory and experiment," *IEEE Trans. Antennas Propagat.*, vol. 59, no. 5, pp. 1438–1445, May 2011.
[7] A. Dadgarpour, M. S. Sorkherizi, and A. A. Kishk, "Wideband low-loss magnetoelectric dipole antenna for 5G wireless network with gain enhancement using meta lens and gap waveguide technology feeding," *IEEE Trans. Antennas Propag.*, vol. 64, no. 12, pp. 5094–5101, Dec. 2016.
[8] H. Attia, M. L. Abdelghani, and T. A. Denidni, "Wideband and high-gain millimeter-wave antenna based on FSS Fabry–Pérot cavity," *IEEE Trans. Antennas Propag.*, vol. 65, no. 10, pp. 5589–5594, Oct. 2017.
[9] A. Hosseini, F. Capolino, and F. De Flaviis, "Gain enhancement of a v-band antenna using a Fabry–Pérot cavity with a self-sustained all-metal cap with FSS," *IEEE Trans. Antennas Propag.*, vol. 63, no. 3, pp. 909–921, Mar. 2015.
[10] N. G. Alexópoulos and D. R. Jackson, "Fundamental superstrate (cover) effects on printed circuit antennas," *IEEE Trans. Antennas Propag.*, vol. 32, no. 8, pp. 807–816, Aug. 1984.
[11] S. Abadal, C. Liaskos, A. Tsioliaridou, A. Tsioliaridou, A. Pitsillides, J. Solé-Pareta, E. Alarcón, and A. Cabellos-Aparicio, "Computing and communications for the software-defined metamaterial paradigm: A context analysis," *IEEE Access*, vol. 5, pp. 6225–6235, 2017.
[12] H. Attia, M. M. Bait-Suwailam, and O. M. Ramahi, "Enhanced gain planar inverted-f antenna with metamaterial superstrate for UMTS applications," *PIERS Online*, vol. 6, no. 6, pp. 585–588, 2010.
[13] S. I. Kwak, D. Sim, J. H. Kwon, and Y. J. Yoon, "Design of PIFA with metamaterials for body-SAR reduction in wearable applications," *IEEE Trans. Electromagn. Compat.*, vol. 59, no. 1, pp. 297–300, Feb. 2017.
[14] T. Zvolensky, J. N. Gollub, D. L. Marks, and D. R. Smith, "Design and analysis of a W-band metasurface-based computational imaging system," *IEEE Access*, vol. 5, pp. 9911–9918, 2017.
[15] O. Yurduseven, D. L. Marks, J. N. Gollub, D. R. Smith, "Design and analysis of a reconfigurable holographic metasurface aperture for dynamic focusing in the Fresnel zone," *IEEE Access*, vol. 5, pp. 15055–15065, 2017.
[16] T. Ueda, K. Okamoto, and T. Itoh, "Enhancement of phase-shifting nonreciprocity in metamaterial lines with comb-shaped capacitive stubs on the normally magnetized ferrite substrate," *IEEE Trans. Magn.*, vol. 54, no. 11, Nov. 2018, Art. no. 2502205.
[17] A. El-Makadema, L. Rashid, and A. K. Brown, "Geometry design optimization of large-scale broadband antenna array systems," *IEEE Trans. Antennas Propag.*, vol. 62, no. 4, pp. 1673–1680, Apr. 2014.
[18] Y. J. Cheng, Y. X. Guo, and Z. G. Lin, "W-band large-scale high-gain planar integrated antenna array," *IEEE Trans. Antennas Propag.*, vol. 62, no. 6, pp. 3370–3373, Jun. 2014.
[19] H. Raza, J. Yang, P.-S. Kildal, and E. Alfonso, "Microstrip-ridge gap waveguide–study of losses, bends, and transition to WR-15," *IEEE Trans. Microw. Theory Techn.*, vol. 62, no. 9, pp. 1943–1952, Sep. 2014.
[20] A. U. Zaman and P.-S. Kildal, "Wide-band slot antenna arrays with single-layer corporate-feed network in ridge gap waveguide technology," *IEEE Trans. Antennas Propag.*, vol. 62, no. 6, pp. 2992–3001, Jun. 2014.
[21] E. Rajo-Iglesias and P.-S. Kildal, "Numerical studies of bandwidth of parallel-plate cut-off realised by a bed of nails, corrugations and mushroom-type electromagnetic bandgap for use in gap waveguides," *IET Microw., Antennas Propag.*, vol. 5, no. 3, pp. 282–289, Feb. 2011.
[22] H. Attia, M. S. Sorkherizi, and A. A. Kishk, "60 GHz Slot Antenna Array Based on Ridge Gap Waveguide Technology Enhanced with Dielectric Superstrate," in *Proc. 9th Eur. Conf. Antennas Propag. (EuCAP)*, Apr. 2015, pp. 1–4.
[23] C. Balanis, *Antenna Theory: Analysis and Design*, 2nd ed. New York, NY, USA: Wiley, 1997.
[24] S. A. Razavi, P. Kildal, L. Xiang, E. Alfonso Alós, and H. Chen, "2×2-slot element for 60-GHz planar array antenna realized on two double-sided PCBs using SIW cavity and EBG-type soft surface fed by microstrip-ridge gap waveguide," *IEEE Trans. Antennas Propag.*, vol. 62, no. 9, pp. 4564–4573, Sep. 2014.
[25] H. Attia and A. A. Kishk, "Transmission line model of RGW slot antenna covered with superstrate at 60 GHz," in *Proc. IEEE Int. Symp. Antennas Propag. USNC/URSI Nat. Radio Sci. Meeting*, Vancouver, BC, Canada, Jul. 2015, pp. 2045–2046.
[26] D. M. Pozar, *Microwave Engineering*, 2nd Ed. New York, NY, USA: Wiley, 1998.
[27] A. E. H. Love, "The Integration of the Equations of Propagation of Electric Waves," *Philos. Trans. Roy. Soc. London. A, Containing Papers Math. Phys. Character*, vol. 197, pp. 287–299, Jan. 1901.
[28] *Symbolic Math Toolbox*. Accessed: Jul. 20, 2019. [Online]. Available: https://www.mathworks.com/products/symbolic.html

HUSSEIN ATTIA was born in Zagazig, Egypt. He received the B.Sc. degree (Hons.) in electronics and communication engineering from Zagazig University, Egypt, in 1999, and the Ph.D. degree in electrical and computer engineering from the University of Waterloo, Waterloo, ON, Canada, in 2011. He was a Research Engineer with the Coding and Signal Transmission Laboratory, University of Waterloo, from 2011 to 2013.

He was granted a Postdoctoral Fellowship at Concordia University, Montreal, QC, Canada, from 2014 to 2015. He was a Visiting Scholar at University de Quebec (INRS), from 2015 to 2017. He is currently an Assistant Professor with the King Fahd University of Petroleum and Minerals (KFUPM), where he is leading a Research Group of four graduate students and one research assistant. He published more than 48 journals and conference papers. His research interests include millimeter-wave high-gain and wide-band antennas, analytical techniques for electromagnetic modeling, and engineered magnetic metamaterials. During the Ph.D. program, he received the University of Waterloo Graduate Scholarship for excellence in research and coursework, in 2009. He was a Finalist in the Student Paper Competition of the 2011 IEEE AP-S International Symposium on Antennas and Propagation.